Spring persistence, transition and resurgence of El Niño

Sang-Ki Lee[1,2], Pedro N. DiNezio[3], Eui-Seok Chung[4], Sang-Wook Yeh[5], Andrew T. Wittenberg[6], and Chunzai Wang[2]

[1]Cooperative Institute for Marine and Atmospheric Studies, University of Miami, Miami, Florida

[2]NOAA Atlantic Oceanographic and Meteorological Laboratory, Miami, Florida

[3]International Pacific Research Center, School of Ocean and Earth Science and Technology, University of Hawaii at Manoa, Honolulu, Hawaii

[4]Rosenstiel School of Marine and Atmospheric Sciences, University of Miami, Miami, Florida

[5]Department of Marine Sciences and Convergent Technology, Hanyang University, Ansan, Korea

[6]NOAA Geophysical Fluid Dynamics Laboratory, Princeton, New Jersey

To be Submitted to Geophysical Research Letters

September 2014

Corresponding author address: Dr. Sang-Ki Lee, CIMAS, University of Miami, 4600 Rickenbacker Causeway, Miami, FL 33149, USA. E-mail: Sang-Ki.Lee@noaa.gov.

Abstract

We present a systematic exploration of differences in the spatio-temporal sea surface temperature (SST) evolution among observed El Niño events. This inter-El Niño variability is captured by two leading orthogonal modes, which explain more than 60% of the inter-event variance. The first mode illustrates the extent to which warm SST anomalies (SSTAs) in the eastern tropical Pacific (EP) persist into the boreal spring after the peak of El Niño. Our analysis suggests that a strong El Niño event tends to persist into the boreal spring in the EP, whereas a weak El Niño favors a rapid development of cold SSTAs in the EP shortly after its peak. The second mode captures the transition and resurgence of El Niño in the following year. An early-onset El Niño tends to favor a transition to La Niña, whereas a late-onset El Niño tends to persist long enough to produce another El Niño event. The spatio-temporal evolution of several El Niño events during 1949-2013 can be efficiently summarized in term of these two modes, which are not mutually exclusive, but exhibit distinctive coupled atmosphere-ocean dynamics.

1. Introduction

Although it has been long recognized that more than one degree of freedom is needed to describe El Niño–Southern Oscillation (ENSO) [*Trenberth and Stepaniak*, 2001], inter-ENSO variability (or ENSO diversity) received renewed attention in recent years. As summarized in two recent review articles [*Capotondi et al*., 2014; *Yeh et al*., 2014], there is a continuum of ENSO spatial patterns of anomalous sea surface temperature (SST), thermocline depth, zonal currents and atmospheric convection. At two extremes of this continuum are the "El Niño Modoki", (also referred to as "Central Pacific El Niño", "Dateline El Niño" and "Warm Pool El Niño" in the literature), which has its peak SST anomalies (SSTAs) in the central tropical Pacific (CP); and the "conventional El Niño" which typically has its peak SSTAs in the eastern tropical Pacific (EP). Since the zonal SST gradient is relatively strong and the thermocline is relatively deep in the CP, the growth of the "El Niño Modoki" relies more on the zonal advection feedback than the thermocline feedback [*Jin and An*, 1999; *Kug et al*., 2010].

ENSO SSTAs tend to peak during boreal winter [*Rasmusson and Carpenter*, 1982]. Thus, the great majority of recent studies on ENSO diversity have focused on the different spatial patterns of ENSO SSTAs during the peak phase in December to February (DJF [0,+1]); hereafter any month in an ENSO onset year is identified by the suffix (0) whereas any month in an ENSO decay year by the suffix (+1). In contrast, inter-event differences in the temporal evolution of ENSO have received much less attention [e.g., *Yu and Kim*, 2010; *Choi et al*., 2013]. However, the onset and decay phases of ENSO typically occurring in boreal spring and summer also play very important roles in forcing climate variability around the globe associated with the East Asian monsoon, tropical cyclones, terrestrial rainfalls and extra-tropical extreme weather events [e.g., *Wu and Wang*, 2002; *Camargo and Sobel*, 2005; *Lee et al*., 2013; 2014].

Therefore, our main goal in this study is to identify and explain the spatio-temporal evolution of inter-El Niño variability in the tropical Pacific for the entire lifespan of El Niño from onset to decay. To achieve this, here we present an objective methodology to identify two leading orthogonal modes of inter-El Niño variability (section 2 and 3). We present possible mechanisms leading to the two orthogonal modes (section 4 and 5) and discussed the occurrence of the two modes in observed El Niño events (section 6).

2. Data and Methods

We explore the spatio-temporal evolution of observed El Niño events in the following datasets. The Extended Reconstructed Sea Surface Temperature version 3b (ERSST3), an in situ analysis of global monthly SST on a 2° longitude by 2° latitude grid [*Smith et al*., 2008] is used to compute SSTAs in the equatorial Pacific for the period of 1949-2013. Two reanalysis products are also used to explore the coupled atmosphere-ocean processes involved with the two orthogonal modes. The Simple Ocean Data Assimilation ocean reanalysis [*Giese and Ray*, 2011] is used to derive the depth of 20ºC isotherm, a proxy for the depth of thermocline. The 20th Century Reanalysis [*Compo et al*., 2011] is used to derive surface wind stress fields.

We identify 21 El Niño events during the period of 1949-2013 based on the threshold that the 3-month averaged SSTAs in Niño 3.4 (120°W–170°W and 5°S–5°N) exceed 0.5°C for a minimum of five consecutive months. There are a few multi-year El Niño events during the study period. They are treated here as multiple El Niño events. For instance, the El Niño that started in the summer of 1986 and continued until the early spring of 1988 is treated as two consecutive El Niño events; that is, the onset and decay of the 1986–1987 El Niño followed by

the onset and decay of the 1987–1988 El Niño. See Figure S1 in the supporting information for details on the individual events included in this analysis.

Next, we construct longitude-time maps of equatorial Pacific SSTAs (averaged between the 5ºS and 5ºN latitude band) for each individual event. The time and longitude axes span from January of the onset year to December of the decay year, and the entire equatorial Pacific (120ºE - 80ºW), respectively. We then perform an Empirical Orthogonal Function (EOF) analysis of these 21 longitude-time maps of equatorial Pacific SSTAs in order to isolate the preferred spatio-temporal modes of inter-El Niño variability. Note that the resulting principal components (PCs) are associated with each individual El Niño event.

By using EOF modes (EOFs) to explore the inter-El Niño variability, we do not mean to imply that there is any multi-modality in the distribution of El Niño events, nor that El Niño events tend to cluster around specific discrete types. The EOFs simply represent a linearly independent set of longitude-time structures that captures the maximum amount of inter-event El Niño variance. As such, they should serve as an efficient basis for describing the continuum of diversity in El Niño evolution.

3. Two Leading Modes of Inter-El Niño Variability

The two leading EOFs are shown in Figure 1b and c along with the composite mean (CM) of the tropical Pacific El Niño SSTAs in Figure 1a. The first and second EOFs represent 34.4% and 27.6% of the total inter-El Niño variance, respectively. Overall, the amplitude of inter-El Niño variability is largest in the decay year after the peak season. This suggests that our attention should be drawn to the post peak season to improve our understanding of inter-El Niño variability.

The first EOF mode (Figure 1b) mainly illustrates inter-event variability of SSTAs in the far eastern tropical Pacific during April, May and June of the decay year (AMJ [+1]) as also evident in Figure 2a. As shown in Figure 2b, the first EOF mode is well correlated with the Niño 3.4 index for the peak season (r = 0.74; significant above 99.9% level). This means that a strong El Niño event tends to persist into the boreal spring in the EP. In contrast, a weak El Niño event favors a rapid development of cold SSTAs in the EP after the peak season and a transition to La Niña. Four El Niño events (1957-1958, 1982-1983, 1991-1992 and 1997-1998) are examples of the former (i.e., strong and persistent). Five other El Niño events (1953-1954, 1963-1964, 1969-1970, 1977-1978 and 1987-1988) fit well with the latter (i.e., weak and early-terminating).

The second EOF mode (Figure 1c) captures inter-event variability in the central and eastern tropical Pacific during October, November and December of the decay year (OND [+1]) as also evident in Figure 2c. Thus, it mainly describes whether El Niño will resurge or transition to La Niña in the following year. Unlike the first mode, this mode is not highly correlated with the SSTAs in Niño 3.4 for DJF (0,+1) (r = 0.49; not significant at 99.9% level; not shown). This means that while a strong (weak) El Niño event does favor a following La Niña (El Niño) event, the peak season strength of El Niño may not be the dictating factor.

Interestingly, the second EOF mode is better correlated with the 20ºC isotherm depth in Niño 3 during JJA (0) as shown in Figure 2d (r = 0.68; significant above 99.9% level). In other words, if a downwelling Kelvin wave train arrives in the EP early in boreal spring and summer to produce an early onset of El Niño, that El Niño event tends to favor a transition to La Niña as it dissipates. On the other hand, if a downwelling Kelvin wave train arrives in the EP late in boreal fall and winter to produce a delayed-onset of El Niño, it tends to favor a subsequent resurgence of the El Niño. This conjecture is indeed supported by our further analysis to be discussed in

section 5. Four El Niño events (1972-1973, 1982-1983, 1987-1988 and 1997-1998) can be considered as the former (i.e., early-onset and transitioning). Only two El Niño events (1968-1969 and 1986-1987) fit with the latter (i.e., late-onset and resurgent).

4. Spring Persistence of El Niño

To better understand the atmosphere-ocean dynamics associated with the first EOF mode, here we explore the longitude-time maps of anomalous SST, 20ºC isotherm depth, and surface wind stress vectors regressed onto PC1. The first EOF mode describes a continuum of El Niño events ranging from those that persist well into boreal spring (PC1 = 1) to those that terminate early and transition to La Niña (PC1 = -1). We analyze both the persistent and early-terminating cases by adding EOF1 to CM and subtracting EOF1 from CM, respectively.

The persisting El Niño case (CM+EOF1) exhibits much stronger SSTAs and deeper thermocline anomalies over the EP during the peak season (Figure 3b) in comparison to CM (Figure 3a). While the climatological SSTs in the EP are generally quite cold near the end of the calendar year, sufficiently strong warm SSTAs in the EP during this time can favor atmospheric deep convection (see Figure S2b) and thus strongly reduce the equatorial easterly trade winds in the CP [*Hoerling et al*., 1997; *Jin et al*., 2003; *Lengaigne and Vecchi*, 2009]. Thus, as illustrated in Figure 3b, the thermocline in the EP further deepens and helps maintain the warm SSTAs in the EP throughout the boreal spring beyond the peak season.

During the second half of the onset year, due to the massive reduction of the easterlies and the associated divergent Sverdrup transport (not shown), a large amplitude upwelling Kelvin wave train emerges in the western tropical Pacific, and then gradually penetrates toward the east in accordance with the behavior of a slow coupled “SST mode” [*Neelin*, 1991]. Consistent with

the recharge-discharge process [*Jin*, 1997; *Meinen and McPhaden*, 2000], the thermocline shoals in the entire tropical Pacific during the second half of the decay year. The transition to La Niña, however, is presumably suppressed by reduced entrainment of subsurface waters into the mixed layer due to a prolonged weakening of the trade winds [*Lengaigne and Vecchi*, 2009].

Consistent with our interpretation of CM+EOF1, the two extreme El Niño events, namely the 1982-1983 and 1997-1998 events, persisted into the boreal spring after the peak season. For these two events, the peak season total SSTs in the EP exceeded the present-day threshold value for deep convection [*Lengaigne and Vecchi*, 2009; *Vecchi and Harrison*, 2006; *Vecchi*, 2006]. However, both of these El Niño events transitioned to La Niña events, unlike the strong and persistent case described by CM+EOF1. This suggests that the 1982-1983 and 1997-1998 events cannot be solely described by CM+EOF1.

As shown in Figure 3c, the early-terminating case (CM-EOF1) describes a weak El Niño that transitions to a La Niña event. This case is characterized by a rapid development of cold SSTAs in the EP shortly after the peak season. Since the climatological SSTs in the EP are quite cold all year long, except in boreal spring, it is unlikely that a weak El Niño can induce deep convection in the EP (see Figure S2c). Therefore, the warm SSTAs in the CP are stronger and more persistent than those in the EP. This in turn induces easterly wind anomalies converging to the CP from the east; thus, the thermocline shoals in the far eastern tropical Pacific and cold SSTAs develop in the EP shortly after the peak season. Since the climatological SSTs in the EP are warmest in boreal spring, the cold SSTAs in the EP could inhibit atmospheric convection (see Figure S2c) and thus reinforce the easterly winds. Therefore, a positive atmosphere-ocean feedback may kick in to further increase the easterly winds, which in turn may further decrease

the thermocline depth in the EP and maintain the cold SSTAs in the EP throughout the decay year (Figure 3c).

Unlike the strong and persistent El Niño case described by CM+EOF1, an onset of the weak and early-terminating El Niño case described by CM-EOF1 cannot be explained by the slow mode. This is more likely to be induced by the zonal advection feedback, which amplifies initial warm SSTAs in the CP generated either locally or remotely [e.g., *Vimont et al*., 2001; *Yu et al*., 2010].

5. Transition and Resurgence of El Niño

As shown in Figure 3e, CM+EOF2 describes an El Niño that transitions to a La Niña event (i.e., transitioning El Niño). An important feature to note is that the thermocline in the far eastern tropical Pacific is already quite deep in the boreal spring of the onset year, suggesting an early arrival of the downwelling Kelvin wave train in the EP. Therefore, the SST and zonal wind stress anomalies are already robust in the boreal spring and early summer of the onset year.

Figure 3e suggests that the onset of La Niña during the decay year is linked to the slow eastward propagation of an air-sea coupled upwelling Kelvin wave train, in accordance with the slow mode. It appears that the early developments of SST and zonal wind stress anomalies in the boreal spring and summer of the onset year increase the *time integral* of the divergent Sverdrup transport prior to and during the peak season, and thus increase the total amount of the warm water discharge (not shown). Therefore, a robust off-equatorial upwelling Rossby wave train is generated and later reflected at the western boundary as an equatorial upwelling Kelvin wave train that in turn slowly penetrates toward the east in accordance with the slow mode. Accordingly, the thermocline shoals and produces the cold SSTAs in the CP during the boreal

summer of the decay year. In turn, the easterly winds increase to the west of the cold SSTAs. This appears to activate a positive atmosphere-ocean feedback, leading to a robust onset of La Niña (see Figure 3e and S3e).

The atmosphere-ocean processes linked to the El Niño-to-La Niña transitions described by CM+EOF2 and CM-EOF1 appear to be entirely different. As discussed earlier, central to the weak El Niño case described by CM-EOF1 are the enhanced easterlies converging from the east toward the CP during and after the peak season, which in turn presumably instigate a positive air-sea feedback to produce and amplify the cold SSTAs in the EP. On the other hand, the robust development and slow eastward-propagation of the air-sea coupled upwelling Kelvin wave train are the key points for the development of La Niña in the early-onset El Niño case described by CM+EOF2.

As shown in Figure 3f (and Figure S3f), CM-EOF2 describes an El Niño event that persists long enough to produce another El Niño event (i.e., resurgent El Niño). In this case, a downwelling Kelvin wave train arrives in the EP late in the boreal fall and winter of the onset year, producing a delayed onset of El Niño. Thus, the SST and zonal wind stress anomalies remain quite weak in the boreal spring and summer of the onset year.

Note that the upwelling Kelvin wave train largely dissipates away before it passes the date line. It appears that the late developments of the SST and zonal wind stress anomalies do not allow enough time prior to and during peak season to discharge the necessary amount of the warm water volume to build a robust upwelling Kelvin wave train in the western tropical Pacific. As a result, the depressed thermocline in the EP dissipates extremely slowly.

The thermocline depth anomalies are quite small beyond the boreal spring of the decay year. Therefore, it is unlikely that the prolonged but weak depression of the thermocline maintains the

warm SSTAs in the CP beyond the boreal spring of the decay year. This suggests that the persistent warm SSTAs in the CP during the second half of the decay year may be maintained by other mechanisms such as the zonal advection feedback or the atmosphere-ocean thermal feedback [*Dommenget*, 2010; *Clement et al*., 2011]. Further analysis of the upper ocean heat budget may shed a light on the mechanism involving the resurgent El Niño case described by CM-EOF2. This is left for future studies.

6. Occurrences of the Two Leading Modes in Observed El Niño Events

Figure 4 shows the normalized PC1 and PC2 for all 21 El Niño events. As shown, some El Niño events are readily characterized by using one of the two EOFs of inter-El Niño variability. For instance, three El Niño events (1953-1954, 1963-1964 and 1969-1970) are clearly weak and early-terminating in the EP (CM-EOF1), whereas the 1972-1973 El Niño event is early-onset and transitioning (CM+EOF2)

For many El Niño events, including most of the strongest ones, both EOFs of inter-El Niño variability are required to characterize them. For instance, the two extreme El Niños, the 1982-1983 and 1997-1998 events, are not only strong and persistent in the EP (CM+EOF1) but also early onset and transitioning (CM+EOF2). It is interesting to note that none of the other 19 El Niño events is characterized in such a combination of the two aspects, suggesting that these two El Niño events are quite unique. Note that such combination of the two aspects is not contradictory. It simply describes that these two El Niño events are both strong and early onset events; thus, they persisted long in the EP until they transitioned to La Niña events.

The 1987-1988 event is also one of a kind. It is not only a weak event but also an early onset event, both of which contribute to its transition to the 1988-1989 La Niña event. Two other El

Niños, the 1968-1969 and 1986-1987 events, persisted into the boreal spring after the peak season in EP. They also persisted long enough to produce the 1969-1970 and 1987-1988 El Niño events. Therefore, these events are both strong and late onset events.

Other El Niño events with their two PC values between -1 and 1, such as the 1951-1952, 1957-1958, 1965-1966, 1994-1995, 2002-2003, 2004-2005, 2006-2007 events, cannot be clearly classified using the two EOFs. This suggests that the spatio-temporal evolution associated with inter-El Niño variability is, to a certain extent, stochastic [e.g., *Lopez and Kirtman*, 2014], supporting the idea of an "El Niño continuum" [*Giese and Ray*, 2011; *Capotondi et al*., 2014].

7. Discussions

Additional analyses are performed to test if and how the two leading EOFs are affected by the SST dataset used and by the criteria for identifying El Niño. First, the Hadley Centre SST data set is used to repeat the inter-El Niño EOF analysis to find two leading EOFs that are almost identical to those derived from ERSST3 (not shown). Four additional El Niños, the 1979-1980, 1990-1991, 1992-1993, 2001-2002, and 2003-2004 events, that are not included in this study, but considered elsewhere [e.g., *Yeh et al*., 2009] are included to repeat the inter-El Niño EOF analysis. In that analysis, the second EOF mode becomes the dominant mode (36.3%) while the first EOF mode becomes the second dominant mode (24.8%). However, the spatio-temporal structures of the two EOFs are almost unaltered (not shown). These results suggest that the two leading EOFs of inter-El Niño variability described in this study are robust features in the available observations. However, given the modulation of ENSO [*Wittenberg*, 2009; 2014; *Collins et al*., 2010; *DiNezio et al*., 2012; *Ogata et al*. 2013], future studies should investigate whether the leading modes of inter-event variation change from epoch to epoch, how they

interact with the background climatology of the tropical Pacific, and how they could respond to future climate change.

The persistence, transition, and resurgence aspects captured by the leading EOFs of inter-El Niño variability are closely related to the emergent time scale and predictability of the ENSO phenomenon. Thus the mechanisms described here connect to a large body of earlier work on the time scale and predictability of ENSO, in which the zonal and meridional structure of the ENSO wind response, and the seasonal timing of stochastic westerly wind events in the west Pacific, were found to strongly affect the period, amplitude, and predictability of ENSO events [e.g., *Kirtman*, 1997; *An and Wang*, 2000; *Capotondi et al*. 2006; *Vecchi et al*. 2006; *Gebbie et al*. 2007]. The present study provides a concise framework for summarizing these effects across multiple El Niño events, which can be used to characterize and compare El Niño behavior.

This study suggests that the peak season strength of El Niño is a predictor for the spring persistence and that the onset timing of El Niño is a predictor for the transitioning and resurgent El Niño. The spatio-temporal evolution of an El Niño event after the peak season is therefore potentially predictable if a seasonal prediction model can reproduce the two EOFs. Therefore, it is important to analyze coupled climate models to test their ability to simulate the two EOFs. Finally, due to the El Niño-La Niña asymmetry [e.g., *Hoerling et al*., 1997; *McPhaden and Zhang*, 2009; *Choi et al*., 2013], it is unlikely that our results specific to inter-El Niño variability can be applied to inter-La Niña variability with reversed sign [*DiNezio and Deser*, 2014]. Given that severe weather events over the U.S. frequently occur during the onset and decay phases of La Niña in boreal spring [*Lee et al*., 2013; 2014], it is important to explore inter-La Niña variability in future studies.

Acknowledgments. We would like to thank Hosmay Lopez and Chris Meinen for their helpful comments. This work was supported by NOAA Climate Program Office through its MAPP program [Grant# NA12OAR4310083] and by the base funding of NOAA AOML.

References

An, S.-I., and B. Wang (2000), Interdecadal change of the structure of the ENSO mode and its impact on the ENSO frequency. *J. Clim.*, *13*, 2044-2055.

Camargo, S. J., and A. Sobel (2005), Western North Pacific tropical cyclone intensity and ENSO, *J. Clim*., *18*, 2996-3006.

Capotondi, A., A. Wittenberg, and S. Masina (2006) Spatial and temporal structure of tropical Pacific interannual variability in 20th century coupled simulations. *Ocean Model.*, *15*, 274-298. doi: 10.1016/j.ocemod.2006.02.004.

Capotondi, A. et al. (2014), Understanding ENSO diversity, *B. Am. Meteorol. Soc.*, In-press.

Choi, K.-Y., G. A. Vecchi, and A. T. Wittenberg (2013), ENSO transition, duration and amplitude asymmetries: Role of the nonlinear wind stress coupling in a conceptual model. *J. Clim.*, *26*, 9462-9476. doi: 10.1175/JCLI-D-13-00045.1.

Clement, A. C., P. DiNezio, and C. Deser (2011), Rethinking the ocean's role in the Southern Oscillation, *J. Clim*., *24*, 4056–4072.

Collins, M. et al. (2010), The impact of global warming on the tropical Pacific and El Niño. *Nat. Geosci.*, *3*, 391-397. doi: 10.1038/ngeo868.

Compo, G. P. et al. (2011), The twentieth century reanalysis project, *Q. J. R. Meteorol. Soc*., *137*, 1–28, doi:10.1002/qj.776.

DiNezio, P. N., B. P. Kirtman, A. C. Clement, S.-K. Lee, G. A. Vecchi, and A. Wittenberg (2012), Mean climate controls on the simulated response of ENSO to increasing greenhouse gases. *J. Clim.*, *25*, 7399-7420. doi: 10.1175/JCLI-D-11-00494.1

DiNezio, P. N., and C. Deser (2014), Nonlinear controls on the persistence of La Niña, *J. Clim*., In-press.

Dommenget, D. (2010), A slab ocean El Niño, *Geophys. Res. Lett*., *37*, L20701, doi:10.1029/2010GL044888.

Gebbie, G., I. Eisenman, A. Wittenberg, and E. Tziperman (2007), Modulation of westerly wind bursts by sea surface temperature: A semistochastic feedback for ENSO. *J. Atmos. Sci.*, *64*, 3281-3295. doi: 10.1175/JAS4029.1.

Giese, B. S., and S. Ray (2011), El Niño variability in simple ocean data assimilation (SODA), 1871–2008, *J. Geophys. Res*., *116*, C02024, doi:10.1029/2010JC006695.

Hoerling, M. P., A. Kumar, and M. Zhong (1997), El Niño, La Niña, and the nonlinearity of their teleconnections, *J. Clim.*, *10*, 1769–1786.

Jin, F.-F. (1997), An equatorial ocean recharge paradigm for ENSO. Part I: Conceptual model, *J. Atmos. Sci*., *54*, 811–829.

Jin, F.-F, and S.-I. An (1999), Thermocline and zonal advective feedbacks within the equatorial ocean recharge oscillator model for ENSO. *Geophys. Res. Lett*., *26*, 2989–2992.

Jin, F.-F., S.-I. An, A. Timmermann, and J. Zhao (2003), Strong El Niño events and nonlinear dynamical heating, *Geophys. Res. Lett*., *30*, 1120, doi:10.1029/2002GL016356.

Kirtman, B. P. (1997), Oceanic Rossby wave dynamics and the ENSO period in a coupled model. *J. Clim.*, 10, 1690-1704.

Kug, J.-S., J. Choi, S.-I. An, F.-F. Jin, and A. T. Wittenberg (2010), Warm pool and cold tongue El Niño events as simulated by the GFDL CM2.1 coupled GCM. *J. Clim.*, *23*, 1226-1239. doi: 10.1175/2009JCLI3293.1.

Lengaigne, M., and G. A. Vecchi (2009), Contrasting the termination of moderate and extreme El Niño events in Coupled General Circulation Models, *Clim. Dyn.*, *35*, 299–313.

Lee, S.-K., R. Atlas, D. B. Enfield, C. Wang and H. Liu (2013), Is there an optimal ENSO pattern that enhances large-scale atmospheric processes conducive to major tornado outbreaks in the U.S.?, *J. Clim.*, *26*, 1626-1642.

Lee, S.-K., B. E. Mapes, C. Wang, D. B. Enfield and S. J. Weaver (2014), Springtime ENSO phase evolution and its relation to rainfall in the continental U.S., *Geophys. Res. Lett.*, *41*, 1673-1680.

Lopez, H., and B. P. Kirtman (2014), Tropical Pacific internal atmospheric dynamics and resolution in a coupled GCM, *Clim. Dyn.*, doi 10.1007/s00382-014-2220-7

McGregor, S., A. Timmermann, M. H. England, O. Elison Timm, and A. T. Wittenberg (2013), Inferred changes in El Niño-Southern Oscillation variance over the past six centuries. *Clim. Past*, *9*, 2269-2284. doi: 10.5194/cp-9-2269-2013.

McPhaden, M. J., and X. Zhang (2009), Asymmetry in zonal phase propagation of ENSO sea surface temperature anomalies, *Geophys. Res. Lett.*, *36*, L13703, doi:10.1029/2009GL038774.

Meinen, C. S., and M. J. McPhaden (2000), Observations of warm water volume changes in the equatorial Pacific and their relationship to El Niño and La Niña, *J. Clim.*, *13*, 3551–3559.

Neelin, J. D. (1991), The slow sea surface temperature mode and the fast-wave limit: Analytic theory for tropical interannual oscillations and experiments in a hybrid coupled model. *J. Atmos. Sci.*, *48*, 584-606.

Ogata, T., S.-P. Xie, A. Wittenberg, and D.-Z. Sun (2013), Interdecadal amplitude modulation of El Niño/Southern Oscillation and its impacts on tropical Pacific decadal variability. *J. Clim.*, *26*, 7280-7297. doi: 10.1175/JCLI-D-12-00415.1.

Rasmusson, E. M., and T. H. Carpenter (1982), Variations in tropical sea surface temperature and surface wind fields associated with the Southern Oscillation/El Niño. *Mon. Wea. Rev.*, *110*, 354-384.

Smith, T. M., R. W. Reynolds, T. C. Peterson, and J. Lawrimore (2008), Improvements to NOAA's historical merged land-ocean surface temperature analysis (1880-2006), *J. Clim.*, *21*, 2283-2296.

Trenberth, K. E., and D. P. Stepaniak (2001), Indices of El Niño evolution, *J. Clim.*, *14*, 1697–1701.

Vecchi, G. A., and D. E. Harrison (2006), The termination of the 1997–98 El Niño. Part I: Mechanisms of oceanic change, *J. Clim.*, *19*, 2633–2646.

Vecchi, G. A. (2006), The termination of the 1997–98 El Niño. Part II: Mechanisms of atmospheric change, *J. Clim.*, *19*, 2647–2664.

Vecchi, G. A., A. T. Wittenberg, and A. Rosati (2006), Reassessing the role of stochastic forcing in the 1997-8 El Niño. *Geophys. Res. Lett.*, *33*, L01706. doi: 10.1029/2005GL024738

Vimont, D. J., D. S. Battisti, and A. C. Hirst (2001), Footprinting: a seasonal link between the mid-latitudes and tropics. *Geophys. Res. Lett.*, *28*, 3923–3926.

Wittenberg, A. T. (2009), Are historical records sufficient to constrain ENSO simulations? *Geophys. Res. Lett.*, *36*, L12702. doi: 10.1029/2009GL038710.

Wittenberg, A. T., A. Rosati, T. L. Delworth, G. A. Vecchi, and F. Zeng (2014), ENSO modulation: Is it decadally predictable? *J. Clim.*, *27*, 2667-2681. doi: 10.1175/JCLI-D-13-00577.1.

Wu, R. and B. Wang (2002), A contrast of the East Asian Summer monsoon-ENSO relationship between 1962-77 and 1978-93, *J. Clim.*, *15*, 3266-3279.

Yeh, S.-W., J.-S. Kug, B. Dewitte, M.-H. Kwon, B. Kirtman, and F.-F. Jin (2009), El Niño in a changing climate, *Nature*, *461*, 511–514.

Yeh, S.-W., J.-S. Kug, and S.-I. An (2014), Recent progress on two types of El Niño: Observations, dynamics, and future changes, *Asia-Pac. J. Atmos. Sci*. *50*, 69-81.

Yu, J.-Y., H.-Y. Kao, and T. Lee (2010), Subtropics-related interannual sea surface temperature variability in the central equatorial Pacific. *J. Clim.*, *23*, 2869–2884.

Yu, J.-Y., and S. T. Kim (2010), Three evolution patterns of Central-Pacific El Niño, *Geophys. Res. Lett*., *37*, L08706, doi:10.1029/2010GL042810.

Figure 1. Time-longitude plots of (a) CM and (b and c) the two leading inter-event EOFs of the tropical Pacific SSTAs averaged between 5°S and 5°N, for 21 El Niños during 1949–2013. Units are in ºC. The dashed gray boxes indicate (a) Niño 3.4 in DJF (0,+1); (b) far eastern tropical Pacific (120°W–80°W and 5°S–5°N) in AMJ (+1); (c) Niño 3.4 in OND (+1).

Figure 2. Scatterplot of (a) SSTAs in Niño 3 (AMJ [+1]) versus PC1, (b) SSTAs in Niño 3.4 (DJF [0,+1]) versus PC1, (c) SSTAs in Niño 3.4 (OND [+1]) versus PC2, and (d) D20 anomalies

in the far eastern tropical Pacific (JJA [0]) versus PC2. The two digit numbers indicate the El Niño onset years. For each plot, the black solid line is the linear regression, whereas the two dashed gray lines show the standard error of the linear regression.

Figure 3. Time-longitude plots of the equatorial Pacific SST (color shade), D20 (contour) and wind stress (vector) anomalies averaged between 5°S and 5°N, for (a, d) CM, (b) CM+EOF1, (c) CM-EOF1, (e) CM+EOF2, and (f) CM-EOF2 of the 21 El Niños during 1949–2013. The units are ºC for SST, m for D20 and dyne cm^{-2} for wind stress. The contour interval for D20 is 3.0m. The longest wind stress vector corresponds to 0.34 dyne cm^{-2}.

Figure 4. Normalized PC1 versus PC2 for all 21 El Niño events. The two digit numbers indicate the El Niño onset years.

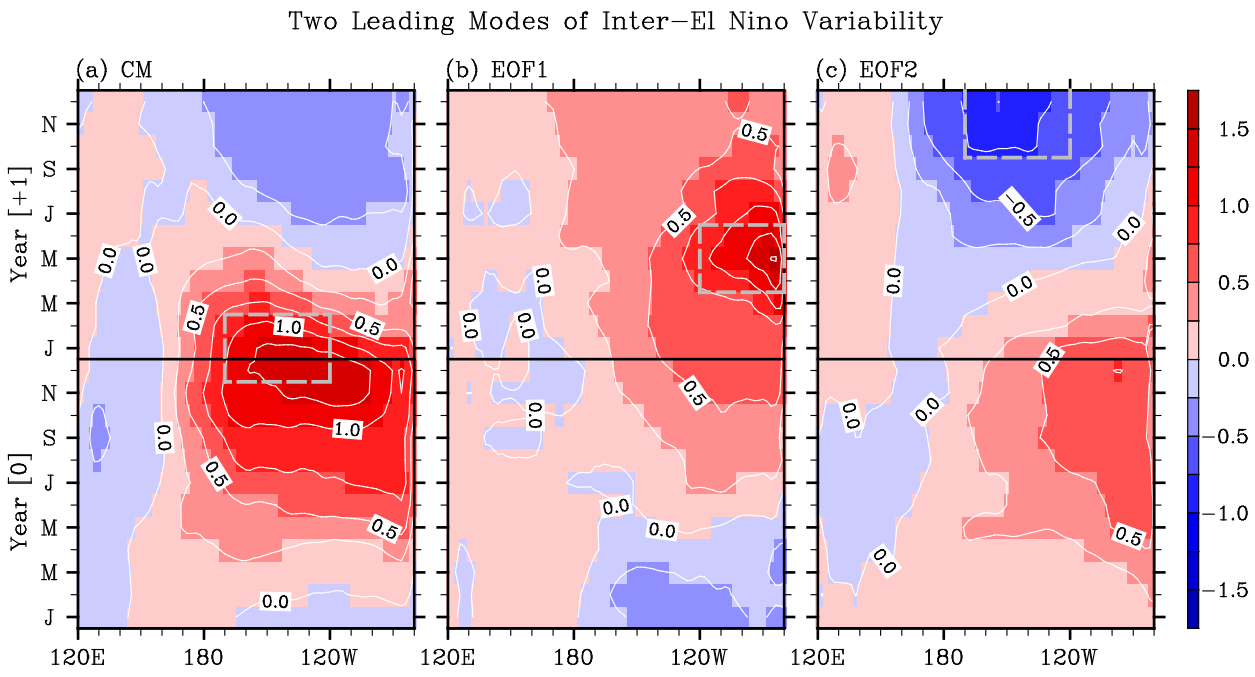

Figure 1. Time-longitude plots of (a) CM and (b and c) the two leading inter-event EOFs of the tropical Pacific SSTAs averaged between 5°S and 5°N, for 21 El Niños during 1949–2013. Units are in ºC. The dashed gray boxes indicate (a) Niño 3.4 in DJF (0,+1); (b) far eastern tropical Pacific (120°W–80°W and 5°S–5°N) in AMJ (+1); (c) Niño 3.4 in OND (+1).

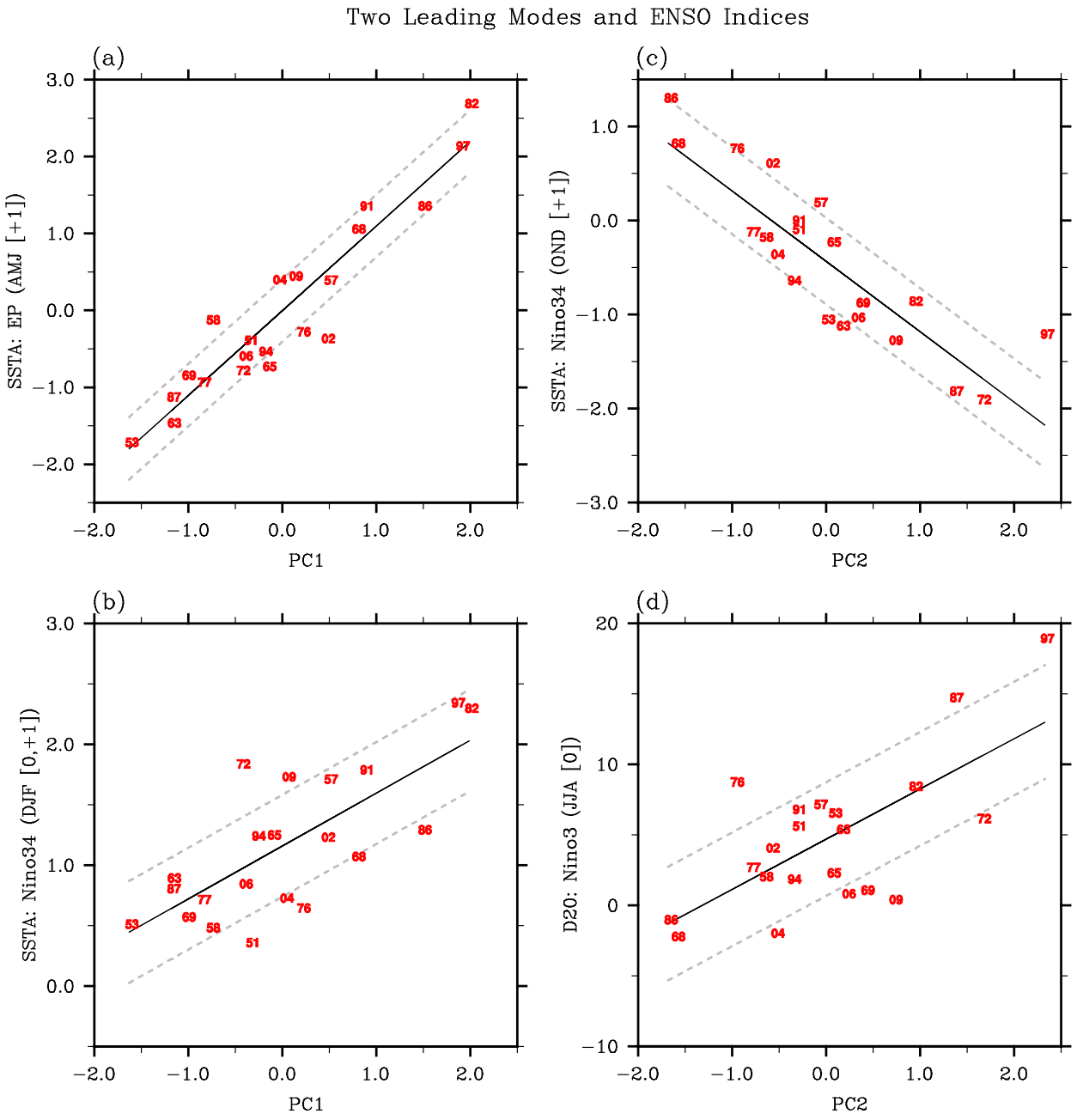

Figure 2. Scatterplot of (a) SSTAs in Niño 3 (AMJ [+1]) versus PC1, (b) SSTAs in Niño 3.4 (DJF [0,+1]) versus PC1, (c) SSTAs in Niño 3.4 (OND [+1]) versus PC2, and (d) D20 anomalies in the far eastern tropical Pacific (JJA [0]) versus PC2. The two digit numbers indicate the El Niño onset years. For each plot, the black solid line is the linear regression, whereas the two dashed gray lines show the standard error of the linear regression.

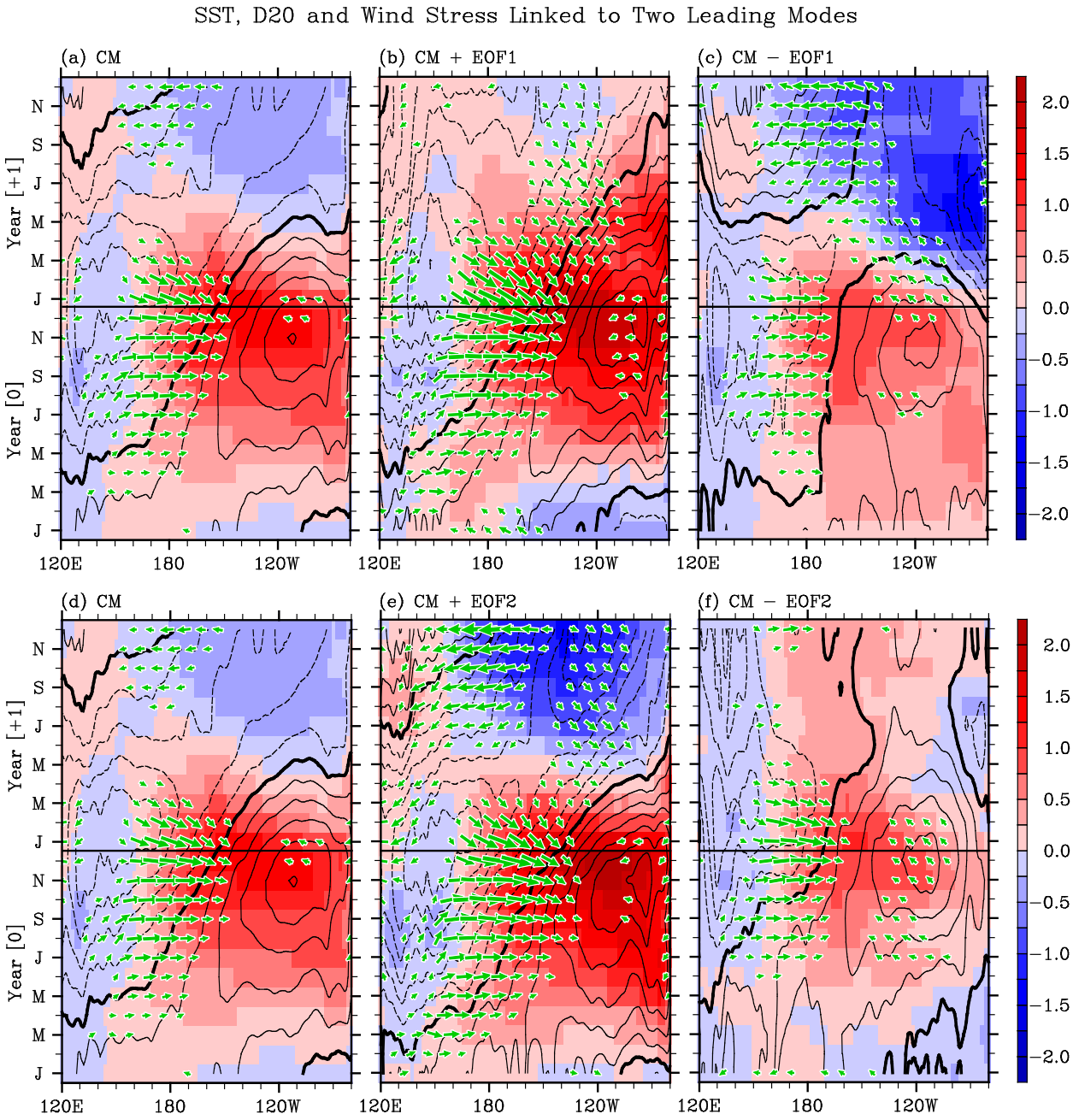

Figure 3. Time-longitude plots of the equatorial Pacific SST (color shade), D20 (contour) and wind stress (vector) anomalies averaged between 5°S and 5°N, for (a, d) CM, (b) CM+EOF1, (c) CM-EOF1, (e) CM+EOF2, and (f) CM-EOF2 of the 21 El Niños during 1949–2013. The units are ºC for SST, m for D20 and dyne cm^{-2} for wind stress. The contour interval for D20 is 3.0m. The longest wind stress vector corresponds to 0.34 dyne cm^{-2}.

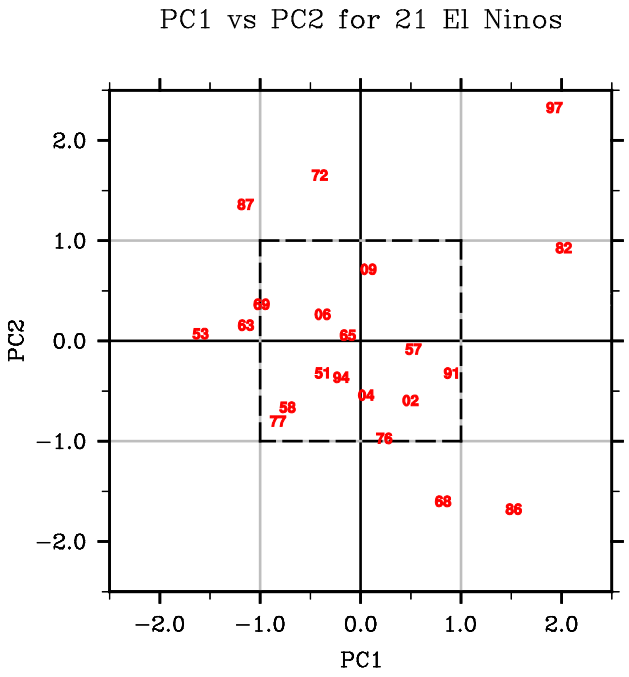

Figure 4. Normalized PC1 versus PC2 for all 21 El Niño events. The two digit numbers indicate the El Niño onset years.